

# FPGA Hardware Neural Control of CartPole and F1TENTH Race Car<sup>0</sup>

Marcin Paluch<sup>\*,‡</sup>, Florian Bolli<sup>\*,‡</sup>, Xiang Deng<sup>\*</sup>, Antonio Rios Navarro<sup>†</sup>,  
Chang Gao<sup>§</sup>, and Tobi Delbruck<sup>\*</sup>

**Abstract**—Nonlinear model predictive control (NMPC) has proven to be an effective control method, but it is expensive to compute. This work demonstrates the use of hardware FPGA neural network controllers trained to imitate NMPC with supervised learning. We use these Neural Controllers (NCs) implemented on inexpensive embedded FPGA hardware for high frequency control on physical cartpole and F1TENTH race car. Our results show that the NCs match the control performance of the NMPCs in simulation and outperform it in reality, due to the faster control rate that is afforded by the quick FPGA NC inference. We demonstrate kHz control rates for a physical cartpole and offloading control to the FPGA hardware on the F1TENTH car. Code and hardware implementation for this paper are available at <https://github.com/SensorsINI/Neural-Control-Tools>.

Keywords: FPGA, NMPC, MLP, multilayer perceptron, neural control, low latency, imitation learning

## I. INTRODUCTION

The idea of using Neural Networks (NN) to model system dynamics for predictive nonlinear control dates to the 1990s [1]–[4]. Vast improvements in Deep Neural Networks (DNN) and Reinforcement Learning (RL) have resulted in impressive demonstrations of direct neural control of difficult nonlinear robotic control problems, e.g. for drone racing [5] and quadruped navigation [6], [7]. Their DNN controllers are trained to infer optimal control actions from the current state and target goals. In this paper, we use the term Neural Controller (NC) to refer to neural networks that directly generate control actions from state and target goals.

An NC maps from a state (or set of past states) and a set of goals to a control action by computing a DNN. The work reported in this paper shows that inexpensive System on Chip (SoC) Field Programmable Gate Arrays (FPGA) can completely offload the control computation with Multilayer Perceptron (MLP) controllers at high control frequency.

Fig. 1 illustrates how we propose to replace a conventional Nonlinear Model Predictive Control (NMPC) controller with a lightweight NC that has been trained in simulation to imitate an expensive NMPC. The NMPC objective used to gather training data is crafted to achieve a desired goal

<sup>0</sup> This work has been submitted to the IEEE for possible publication. Copyright may be transferred without notice, after which this version may no longer be accessible.

<sup>‡</sup> Contributed equally to this work by doing the bulk of development and experiments.

<sup>\*</sup> Sensors Group, Inst. of Neuroinformatics, UZH-ETH Zurich; <https://sensors.ini.ch>.

<sup>†</sup> U. of Seville; [https://investigacion.us.es/sisius/sis\\_showpub.php?idpers=20628](https://investigacion.us.es/sisius/sis_showpub.php?idpers=20628).

<sup>§</sup> TU Delft; <https://www.tudemi.com/>.

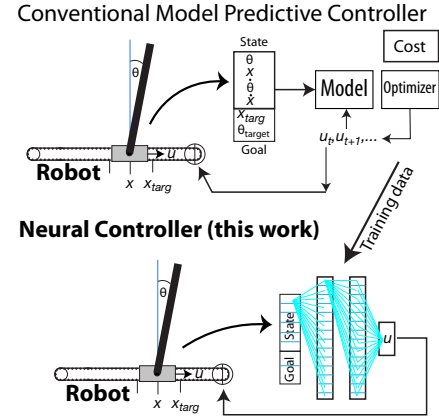


Fig. 1: A lightweight hardware accelerated neural controller replaces a conventional expensive NMPC controller. In this work, the NC is trained by data collected from the NMPC in simulation.

over its rollout horizon. Like with NMPC, implicit feedback control occurs at every timestep.

Our approach follows previous work on hardware accelerated NMPC [3], [8]–[10] but is distinguished by being a pure NC that infers the optimal control from what it has learned in simulation, rather than solving a constrained nonlinear optimization problem at each time step. The DNN requires many mathematical operations per time step, but is accelerated using an open framework for hardware NNs developed by the particle physics community for MLPs [11]. This approach enables quicker control than with NMPC, at least in some scenarios leading to smoother control and faster corrections.

The complete controller is implemented on an entry-level USB-powered FPGA SoC board that costs about \$300 and burns less than 3W. It runs the multilayered NNs with thousands of parameters in microseconds by massive parallelization of the Multiply-Accumulate (MAC) operations. This forms the complete standalone controller for our cartpole, and it is a hardware node in our more complex F1TENTH race car autonomous driving system stack.

## A. CONTRIBUTIONS AND NOVELTY

- 1) We contribute an open source framework<sup>1</sup> for the training and implementation of NMPC neural imitators on FPGA accelerated NCs.

<sup>1</sup><https://github.com/SensorsINI/Neural-Control-Tools>

2) We contribute concrete implementations of hardware NCs for cartpole and F1TENTH, demonstrating their equivalent control performance to NMPC with less power and latency. The hardware cartpole NC matches the NMPC control performance but allows controlling the cartpole at 1 kHz. The F1TENTH NC nearly matches the control performance (laptime) of the NMPC controller in simulation. On the physical car—where we cannot compute the original NMPC sufficiently quickly—it offloads all control computation to the SoC FPGA. We show that it achieves more precise tracking and laps that are completed 20% faster than an optimized pure pursuit controller.

## II. RELATED WORK

There is considerable literature on hardware-accelerated solution of NMPC optimization: Quadratic Programming (**QP**) methods [12], Interior Point (**IP**) [13]–[16], fast gradient and Alternating Direction Method of Multipliers (**ADMM**) [17]–[19], Particle Swarm Optimization (**PSO**) [9], and others [20].

QP solves convex optimization, especially quadratic functions. Sequential Quadratic Programming (**SQP**) is an iterative process that linearizes a nonlinear function and turns it into a sequence of QP optimizations. SQP, the dominant solver used for NMPC, is difficult to parallelize in hardware and is also dependent on correctly adjusting many parameters. NCs are a simpler solution that leverages offline NMPC for simpler implementation of nonlinear optimal control.

We could find only few reports of prior hardware NCs. Diadati [21] mimicked a Proportional Derivative (**PD**) power supply controller with a custom FPGA implementation of a tiny Single Layer Perceptron (**SLP**) with only 5 hidden units. Wang [8], [22] proposed ANN-MPC (analog neural network MPC) to control a power converter by training a similar 5-hidden-unit SLP with transfer learning to mimic the original NMPC. Dong [23] considered simulated drone standoff tracking (flying in circles) and implemented a NC using a 2-layer 100 units per layer MLP on a \$1,500 FPGA. The most closely related work is [10], which demonstrated the use of an open source Recurrent Neural Network (**RNN**) [24] trained to imitate a PD leg prosthetic controller for the knee and ankle joint torques.

## III. METHODS

### A. Neural Controller Accelerator

Our NCs are implemented on a Zynq-7020 SoC hosted on a Zybo Z7-20 development board<sup>2</sup>. This SoC combines a Processing System (**PS**) and Programmable Logic (**PL**) on one chip. The Zynq-7020 includes a 12-bit Analog to Digital Converter (**ADC**) and other peripherals like full-speed USB serial port. Zybos’s 6-pin PMOD connectors simplify connections to external hardware and we use them to communicate with our cartpole robot. The PS (667 MHz dual

<b>Cartpole</b>		
Arch.	MLP 7-32-32-1	
# Params	1,345	
Input Quant.	Q12.2	
Act. Fnc.	tanh	
Weight Quant.	Q14.4	
Act. Quant.	Q12.1	
Intermediate results	up to 18 bits	
Utilization (LUT,FF,BRAM,DSP)	50%, 22%, 11%, 18%	
Compute latency (Vivado estim.)	91 cycles, 3.64 $\mu$ s	
Power consum. (Vivado estim.)	12 mW	
<b>F1TENTH</b>		
Arch.	MLP 64-64-64-2	
# Params	16,778 (incl. $\approx$ 80% zeros)	
Input Quant.	Q16.4	
Act. Fnc.	tanh	
Weight Quant.	Q16.4	
Act. Quant.	Q16.4	
Intermediate results	up to 16 bits	
Utilization (LUT,FF,BRAM,DSP)	64%, 28%, 16%, 24%	
Compute latency (Vivado estim.)	93 cycles, 3.72 $\mu$ s	
Power consum. (Vivado estim.)	13 mW	

TABLE I: NC parameters, PL utilizations, and latencies.

core Cortex-A9 processor) runs a bare metal C program that interfaces the cartpole robot or the F1TENTH car computer to the NC implemented on the FPGA fabric. We designed peripheral PL components (Pulse Width Modulation (**PWM**), ADC, Encoder, Median Filter) with Xilinx Vivado High Level Synthesis (**HLS**).

We used the hls4ml framework<sup>3</sup> to synthesize the MLPs for our NCs. We trained the MLPs using QKeras<sup>4</sup>, a quantized version of Keras. In QKeras, layers are specified as in Keras, but the layer specification includes the quantization of weights and activations. We provide these as QM.N fixed point numbers with M total bits and N-bit integer part including sign bit.

Table I lists the MLP parameters used for the cartpole and F1TENTH NCs, the PL utilization, and the compute latency. We were mainly constrained by the number of LUTs and DSPs. The demand for DSPs can be easily traded against latency, but the usage of LUTs correlates strongly with the network weights and this forced us to experiment with smaller networks, quantization-aware training, and pruning. By rewarding weight pruning in training, we achieved a sparsity of 80% for the F1TENTH NC. Since zero weights do not consume LUTs, it makes the implementation of this larger network possible. We were constrained by development time and are aware that more optimization (particularly for weights) would be beneficial. Both NCs complete an inference step in less than 4  $\mu$ s; for the F1TENTH NC the MACs are computed by parallelism at about 4.5 GOp/s at a clock frequency of only 25 MHz.

### B. Non-linear MPC

NMPC computes a feedback control input  $u_k = \mu(\hat{x}_k)$  by minimizing cost J over a finite horizon of  $N$  steps. Let  $\bar{u}_{k:k+N-1}$  denote an input plan along the MPC horizon of  $N$  timesteps starting from control iteration  $k$ , and  $\hat{x}_{k:k+N}$

<sup>2</sup><https://digilent.com/reference/programmable-logic/zybo-z7/start>

<sup>3</sup><https://github.com/fastmachinelearning/hls4ml>

<sup>4</sup><https://github.com/google/qkeras>

the resulting state trajectory according to the approximated model  $\hat{f}$  of system  $f$ . Then, the solution control input plan  $\nu_{k:k+N-1}$  is

$$\nu_{k:k+N-1} = \underset{\bar{u}_{k:k+N-1} \in \mathcal{U}^N}{\operatorname{argmin}} \left[ J(\hat{x}_{k:k+N}, \bar{u}_{k:k+N-1}) \right] \quad (1)$$

subject to

$$\begin{aligned} \hat{x}_{k+i+1} &= \hat{f}(\hat{x}_{k+i}, \bar{u}_{k+i}) \\ \hat{x}_{k+i} &\in \mathcal{X}, \quad \bar{u}_{k+i} \in \mathcal{U}, \quad i = 0, \dots, N-1 \end{aligned}$$

The control taken for the next time step is then  $\mu(\hat{x}_k) = \nu_k$ .

The cost function  $J$  is crafted to obtain a desired objective. Its terms are usually quadratic and positive definite, but it can also contain extremely nonlinear indicator function terms that specify constraints, such as motor saturation, obstacles, and track edges.

To solve the optimization problem in (1) we used the Resampling Parallel Gradient Descent (**RPGD**) solver from [25]. We used a desktop PC with Intel Core i7-4790K CPU (4GHz, total power  $\approx 150$  W).

### C. Cartpole

Fig. 2A shows the physical cartpole<sup>5</sup> together with the SoC FPGA board that runs the NC. The SoC includes a 12-bit ADC which we run with sampling rate about 350kHz with an additional analog RC filter ( $\tau = RC = 0.1$  ms) and a rolling 64-sample window median filter on FPGA. The cart motor is controlled by PWM FPGA output that drives the motor H-bridge (TB6612FNG) with 10kHz pulses. The motor encoder has 1200 counts per revolution of the gearbox's output shaft, resulting in 118.8 counts per centimeter. The sensor quantization noise is a major obstacle to demonstrate high frequency control - it amplifies while calculating derivatives over short time windows. Hence also for 1kHz NC we average cart velocity and pole's angular velocity resulting in additional 5ms delay for these state components.

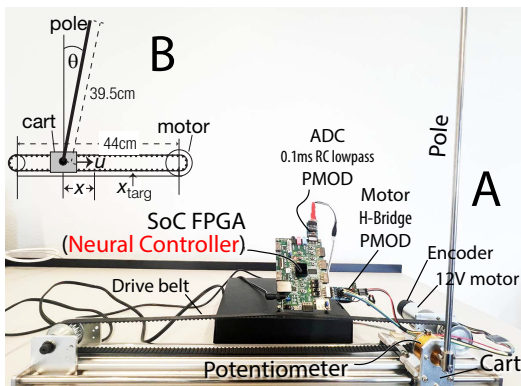


Fig. 2: **A:** Physical cartpole and neural controller hardware. **B:** Cartpole state variables

1) *Cartpole Dynamics:* Fig. 2B illustrates the cartpole state variables. The goal of the cartpole is to swing up the pole and then hold  $\theta = 0^\circ$  (or  $\theta = 180^\circ$ ) while controlling the cart to a target cart position  $x_{\text{targ}}$  using only horizontal cart acceleration  $u$ , as quickly as possible, with the least pole motion, cart position error, motor power, and without hitting track boundaries. The cartpole is underactuated, because it must control pole angle and cart position using a single motor. Cartpole maneuvers require a nonlinear controller, because of the pole dynamics and the constraints on cart position and motor saturation.

2) *NC architecture:* The NC takes as the input state — sine and cosine of the pole angle, angular velocity, cart position and velocity — and target — cart target position and pole target equilibrium — either up and down. While stabilizing pole down is an easier task, it helps quickly reset the cartpole between experiments and demonstrates that the NC can learn two discrete modes of control (with completely opposite signs of small-angle error correction gain), gated by the binary  $\theta_{\text{targ}}$  input. The network outputs normalized motor command. It has 2 hidden layers, 32 units each.

3) *NC data collection and training:* We simulated the cartpole using the differential equations of Green [26]. These equations are integrated using the standard Euler method with intermediate time steps of 2ms. The cart acceleration is calculated by NMPC and updated every 20ms, both in simulation and in our experiments with physical setup. We used RPGD [25] as the optimizer. The controller ran at 50 Hz with a horizon of 35 time steps (0.7s). The cost function contains (weights in brackets) the square penalties on the two minus cosine of the angle (200), angular velocity (13), normalized control signal magnitude (10) and approach to track boundary (active on the extreme 15% of the track, normalized by track length, 100 000) and linear cost on distance to target position (normalized by track length, 80). During the simulated experiments, we change the target position, stabilize at the up and down equilibria, and add known control noise to collect a diverse dataset. We collected 1h of simulated data. After data collection we applied state quantization simulating sensor resolution and mixed the dataset with its own copy with 20ms shifted angle and position derivatives to robustify NCs against delays.

### D. FITENTH car

The FITENTH car is a 1/10 scale autonomous race car. Our goal for this paper is to race it around a track reliably and precisely with a minimum lap time.

For both simulated and physical experiments, we used a commercial indoor RC race track where the extracted map formed the basis for simulations. This racetrack is sticky, with an estimated friction coefficient of about 1.1. An amateur (one of us) can achieve about 24s lap times. The desired race line (minimum curvature line around the given track with a safety margin) was calculated offline with [27] and saved as a set of waypoints. Each waypoint is represented by 3 values: the position (position<sub>x</sub>, position<sub>y</sub>) and the suggested longitudinal velocity  $v_x$ . To control the

<sup>5</sup><https://aliexpi.com/3fGL>: Linear Inverted Pendulum

overall speed of the car, we use a speed factor  $F$  that multiplies  $v_x$  at each waypoint.  $F$  allows us to easily adjust the car’s speed to balance speed and safety.

1) *Simulated F1TENTH Car*: We used a simulated environment for the F1TENTH car called F1TENTH Gym [28]. The car dynamics are based on the Single-Track car model of the CommonRoads Vehicle Models [29]. For every experiment, the car is initialized at a random position on the minimum-curvature race line, pointing along the race line. To model an estimated 80 ms delay in perception and actuation, we implemented a control delay from state measurement to actuation in simulation.

2) *Physical F1TENTH Car*: Fig. 3 shows the physical F1TENTH car and the racetrack. The car is a 1/10 scale Traxxas Slash RC car based on the standard F1TENTH car<sup>6</sup>, carrying an NVIDIA Jetson TX2 as the main computer, a Hokuyo LiDAR (10m, 40Hz), a Bosch BNO-6 IMU and a VESC MK6 (electronic speed controller for the brushless motor). We added the NC Zybo Z7 SoC FPGA of Section III-A.

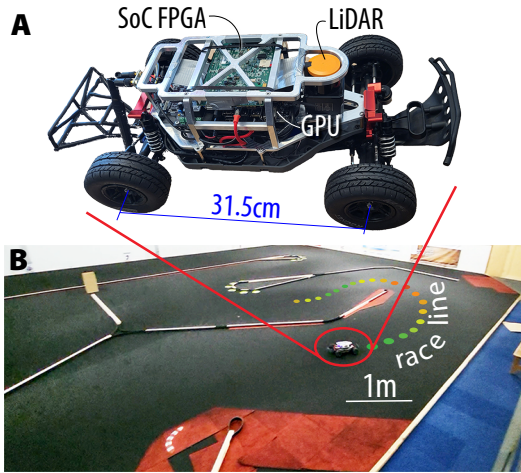


Fig. 3: **A**: F1TENTH car. **B**: Racetrack (RCA2) including an example of the 20 next waypoints of the race line. The suggested speed is color coded (green: faster, red: slower)

The state estimation stack consists of an extended Kalman Filter<sup>7</sup>, which fuses the motor encoder information with the IMU measurement to obtain odometry information. The odometry position estimation is accurate for a short time window, but it drifts over time due to the differential nature of the IMU. To correct the drifting odometry, the AMCL<sup>8</sup> particle filter is used to estimate the car’s position such that the LiDAR scans match the known environment. The map was recorded with the ROS-Cartographer<sup>9</sup> SLAM algorithm.

The car’s linear and angular velocity  $v_x$  and  $\omega_z$  are obtained directly from the Kalman Filter. The steering angle  $\theta$  is calculated by the steering control  $u_{steering}$  and the servo

<sup>6</sup><https://f1tenth.org/build.html>

<sup>7</sup>[http://wiki.ros.org/robot\\_pose\\_ekf](http://wiki.ros.org/robot_pose_ekf)

<sup>8</sup><https://wiki.ros.org/amcl>

<sup>9</sup><https://google-cartographer-ros.readthedocs.io/en/latest/>

model introduced in [28]. The physical car’s slipping angle  $\beta$  is approximated as 0, which is justified by the observation that the car rolls over before slipping due to the track’s high friction.

3) *NC data collection and training*: To train our NC, we used the NMPC controller to collect state-action pairs from the RCA1 track in Fig. 3A. We used RPGD [25] as the optimizer for our simulated NMPC control experiments. The controller ran at 50Hz with a horizon of 20 time steps or 0.4s. It accessed the car’s full state as well as the next 8m of the race line (20 waypoints, including suggested speed, multiplied by the tunable speed factor  $F$ ) as illustrated in Fig. 3.

The cost function for NMPC contains following terms (weights in brackets): the quadratic difference between the car’s position and the desired race line (20.0), the quadratic difference between the car’s speed and the suggested speed of the previously calculated race line (0.1), the car’s steering angle (30.0), the car’s slipping angle (0.01), the first (0.4) and second derivative (10.0) of the steering history.

To compensate for the car’s 80 ms perception+actuation delay, rather than executing  $v_k$  of the NMPC’s optimal control sequence Eq. (1), we executed  $v_{k+4}$  (4/50Hz=80ms). Like this, we execute the control that was calculated for the car’s estimated state 80ms in the future.

We collected this training data in simulation by driving around the Fig. 4A track with the NMPC for 600s for each speed factor  $F \in [0.5, 0.6, 0.7, 0.8, 0.9, 1.0, 1.1, 1.2]$ , so the training data consisted of 4,800s, or 240,000 samples.

The track layout (RCA1 in Fig. 4A) used for training is different than the one used for testing (RCA2 in Fig. 4B). This shows that the NC can generalize over different tracks.

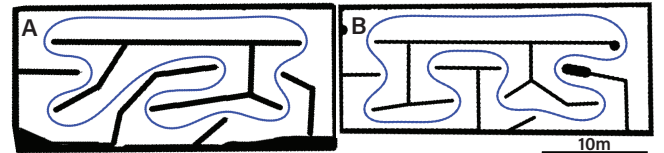


Fig. 4: Maps recorded by the physical car with their minimum curvature race lines. **A**: RCA1, the map used for training, **B**: RCA2, the map used for experiments

4) *NC architecture*: Table I lists the F1TENTH NC parameters. In total, the NC has 64 inputs and 2 outputs. There are 2 hidden layers, each with 64 units.

The inputs of the car NC consist of the next 20 waypoints relative to the car’s position and heading, as described in Section III-D.3, the car’s longitudinal velocity  $v_x$ , angular velocity  $\omega_z$ , steering angle  $\theta$  and slipping angle  $\beta$ . The car’s position and heading are used to convert the waypoints to the car’s relative coordinate system but they are not part of the neural network input.

The NC outputs are the desired longitudinal velocity  $u_{vel}$  and the desired steering angle  $u_\theta$  of the car. The motor throttle is determined from  $u_{vel}$  by the internal PID controller of the VESC. The steering servo receives the desired angle  $u_\theta$

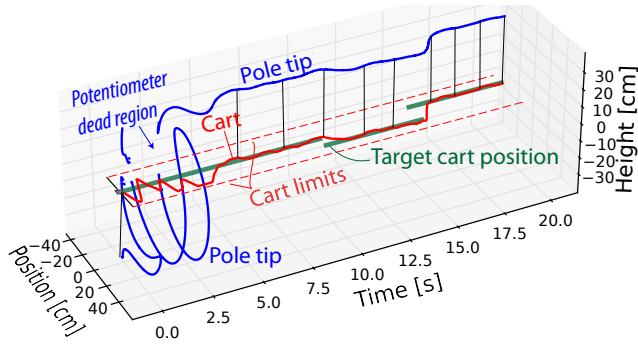


Fig. 5: **Physical cartpole experiment.** The cart and pole tip positions are plotted over time for a swing-up followed by changes in the target cart position. The cartpole is controlled by the hardware NC.

and applies it with its internal PID controller on the steering wheels.

To train a functional NC, we found it was essential to take into account the NMPC's delay compensation. We therefore also trained the NC to output the future control step  $\nu_{k+4}$  exactly like the NMPC.

#### 5) Reference solutions:

- **NMPC:** We used the NMPC from Section III-D.3 as the reference controller for optimal control.
- **Pure Pursuit (PP) Controller:** As a simpler and more computationally efficient reference controller, we used an implementation of PP [30]. PP is widely used in the F1TENTH competition due to its simplicity. The controller can be tuned easily, but it is not able to drive more complex maneuvers such as slipping or drifting. In our work we use a PP with a dynamic look-ahead distance  $d_l$  proportional to the speed of the car with an empirically obtained proportionality factor (0.4). This formulation delivers a short  $d_l$  (accurate tracking) in sharp curves and a larger  $d_l$  (more stable) in high-speed sectors.

## IV. EXPERIMENTAL RESULTS

This section presents the results of our experiments with the physical cartpole and the F1TENTH race car.

### A. Physical Cartpole Experiments

Fig. 5 shows a swing-up followed by changes in target cart position for the physical cartpole of Section III-C. We can observe that the swing-up completes in about 2.5s. Changes in target cart position are accurately tracked.

Fig. 6 compares the cartpole dynamics controlled by the hardware NC at 1 kHz and controlled by NMPC running on a host computer at 50 Hz. The controllers have similar control performance, however, in the inset (\*), we can see that the NC reacts more quickly to the step change of target position. The NC pole error is also smaller (+).

### B. Simulated F1TENTH Car Experiments

This section compares the NC with the original NMPC, and a PP controller. For all car experiments, the speed factor

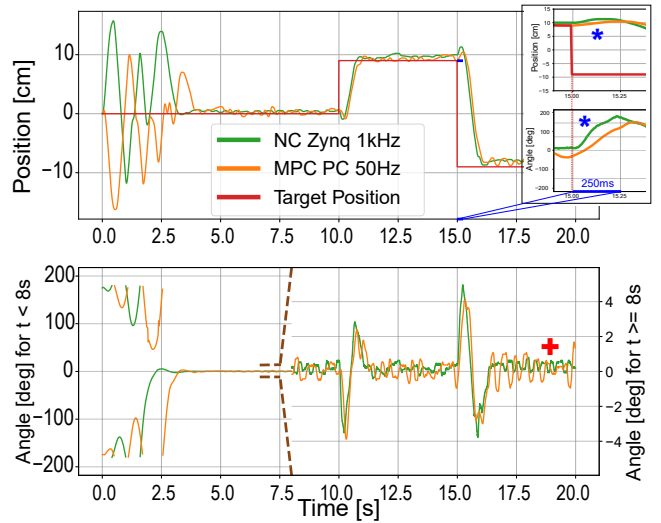


Fig. 6: Comparison of cartpole dynamics with various controllers.

TABLE II: Simulation F1TENTH lap times and position accuracy.

Controller	$F$	$d_{max}$ [m]	$d_{mean}$ [m]	$t_{lap}$ [s]
PP	0.8	0.758	0.188	23.124
NMPC	1.2	0.453	0.048	15.822
NC	1.1	0.317	0.086	17.51

$F$  was experimentally adjusted as high as possible such that the car still could complete 10 laps in a row without crashing.

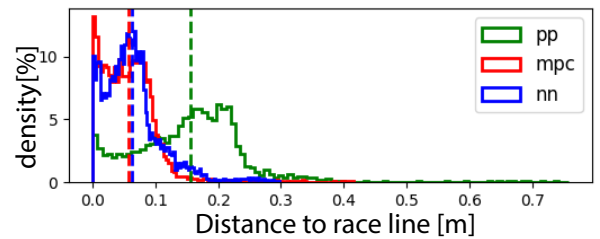


Fig. 7: Histograms of distance errors to minimum curvature race line of all controllers, evaluated in the simulated environment See Table II.

Table II summarizes the maximal 10-lap ( $d_{max}$ ) and the mean ( $d_{mean}$ ) distance to the race line as well as the achieved mean lap time ( $t_{lap}$ ) of each controller. Fig. 7 compares 10 simulated lap tracking error histograms from PP, NMPC, and the NC. The NC drove most precisely. The PP was 30% slower than the NC. The NMPC controller drove fastest and with smallest mean error, but the NC had the smallest maximum error and was slower by only 10% than the NMPC.

### C. Physical F1TENTH Car Experiments

On the physical F1TENTH car, we compared the hardware NC against a PP controller. All results were measured with the state estimation stack described in Section III-D.2.

The NMPC was not able to complete laps with the physical car due to the lack of onboard computational power: The

NMPC ran at a maximum of 10Hz, but only by consuming all the computational resources needed by the state estimation stack.

Table III compares the the performance metrics as in Table II over 10 laps.

Fig. 8 compares 10 lap trajectories of the physical car controlled by the PP controller and the NC. The arrows ( $\rightarrow$ ) show regions where our NC noticeably outperforms the reference PP in terms of accuracy. We suspect that in regions marked by (\*), the recorded trajectory deviates noticeably from the ground truth. The state estimation stack might be inaccurate at high speed or high angular velocity.

Fig. 9 illustrates the according tracking error histograms from PP and the NC.

The NC lap times are 20% quicker than the PP times. The NC tracks the race line more precise than the PP. The PP overshoots the optimal line more than the NC, particularly on sharp curves.

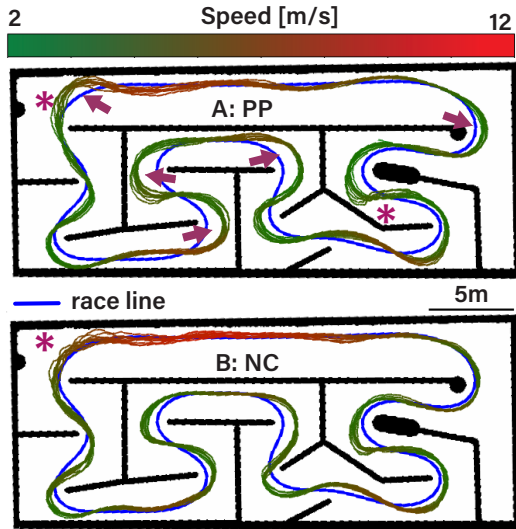


Fig. 8: Trajectories of the physical car controlled with **A**: Pure Pursuit and **B**: NC following minimum curvature race line. See Table III.

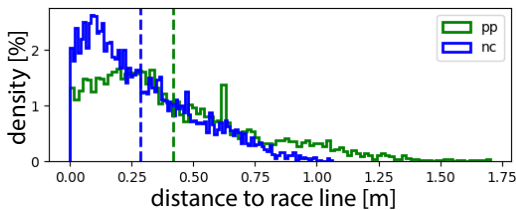


Fig. 9: Histograms of distance errors to minimum curvature race line of the PP and NC controllers on the physical car. See Table III.

## V. CONCLUSION

For the cartpole robot, we showed that the hardware NC achieves control performance that matches the expensive NMPC. The SoC FPGA forms the complete controller of

TABLE III: Physical F1TENTH car lap times and position accuracy.

Controller	$F$	$d_{\max}$ [m]	$d_{\text{mean}}$ [m]	$t_{\text{lap}}$ [s]
PP	0.71	1.80	0.453	24.35
NC	<b>0.86</b>	<b>1.098</b>	<b>0.326</b>	20.04

the system including the sensor and the motor interface. The hardware NC enables a control rate of 1 kHz, which through quick corrections helps reducing angle deviation around equilibrium.

In the F1TENTH car simulation, we showed that the hardware NC follows the race line more accurately and achieves faster lap times than the reference pure pursuit controller. We showed that it competes with its teacher NMPC in terms of accuracy and lap times with a small fraction of the computational effort and latency. The NC can generalize and complete laps on a track with a different distribution of curves than the one it was trained on.

In the physical car, we demonstrated a real-world application that offloads all the control computation onto a low-power and low-cost SoC FPGA. While the NMPC can not be solved in real time on the car’s computer, the hardware NC is able to imitate it and therefore outperforms (in accuracy and lap times) the reference pure pursuit controller.

### A. Limitations and Outlook

Like NMPC, our NCs control performance is degraded by Sim2Real model mismatch. This limitation could be addressed by training with domain randomization as is done in RL [31].

NCs provide a framework to infer state components and environmental variables that are not directly accessible during controller operation. An example is Rapid Motor Adaptation (**RMA**) in [32] or the teacher-student RL method used in [7]. In the same way, if we provide sufficient temporal context, it may be possible to train the NCs for our robots with variable physical properties, such as pole lengths or track frictions. These and similar methods might be useful for car control in the absence of slip angle information which is difficult to measure. This would show further advantages of NCs.

The hardware NCs are not restricted to imitate NMPC controllers with the small MLPs we needed for this work and can easily be adapted to run large RNNs [24] or MLPs [33] trained by other methods.

## ACKNOWLEDGMENTS

This work was supported by the Swiss NSF projects SCIDVS (200021\_185069) and VIPS (40B2-0\_181010) and by the Samsung Global Research Neuromorphic Processor Project (NPP). We thank Daniel Schüpbach for allowing us to use his indoor track in the RC Arena in Gachnang, Switzerland. We thank our students Jago Iranyi, Nigalsan Ravichandran and Eike Himstedt for exploring the topics of this work with us. We thank Pehuen Moure, Ilya Kiselev, and Shih-Chii Liu for helpful comments and the 2023 Telluride Neuromorphic Workshop (<https://tellurideneuromorphic.org>) for the opportunity to develop this work.

## REFERENCES

- [1] N. Bhat and T. J. McAvoy, "Use of neural nets for dynamic modeling and control of chemical process systems," *Comput. Chem. Eng.*, vol. 14, no. 4, pp. 573–582, May 1990, ISSN: 0098-1354. DOI: 10.1016/0098-1354(90)87028-N.
- [2] K. Narendra and K. Parthasarathy, "Identification and control of dynamical systems using neural networks," *IEEE Trans. Neural Netw.*, vol. 1, no. 1, pp. 4–27, Mar. 1990, ISSN: 1045-9227. DOI: 10.1109/72.80202.
- [3] J. Saint-Donat, N. Bhat, and T. J. McAvoy, "Neural net based model predictive control," *Int. J. Control.*, vol. 54, no. 6, pp. 1453–1468, Dec. 1991, ISSN: 0020-7179. DOI: 10.1080/00207179108934221.
- [4] A. Draeger, S. Engell, and H. Ranke, "Model predictive control using neural networks," *IEEE Control Syst. Mag.*, vol. 15, no. 5, pp. 61–66, Oct. 1995, ISSN: 1066-033X, 1941-000X. DOI: 10.1109/37.466261.
- [5] E. Kaufmann, L. Bauersfeld, A. Loquercio, M. Müller, V. Koltun, and D. Scaramuzza, "Champion-level drone racing using deep reinforcement learning," en, *Nature*, vol. 620, no. 7976, pp. 982–987, Aug. 2023, ISSN: 0028-0836, 1476-4687. DOI: 10.1038/s41586-023-06419-4.
- [6] T. Miki, J. Lee, J. Hwangbo, L. Wellhausen, V. Koltun, and M. Hutter, "Learning robust perceptive locomotion for quadrupedal robots in the wild," en, *Sci Robot*, vol. 7, no. 62, eabk2822, Jan. 2022, ISSN: 2470-9476. DOI: 10.1126/scirobotics.abk2822.
- [7] J. Lee, J. Hwangbo, L. Wellhausen, V. Koltun, and M. Hutter, "Learning quadrupedal locomotion over challenging terrain," en, *Sci Robot*, vol. 5, no. 47, Oct. 2020, ISSN: 2470-9476. DOI: 10.1126/scirobotics.abc5986.
- [8] D. Wang, Z. J. Shen, X. Yin, et al., "Model predictive control using artificial neural network for power converters," *IEEE Trans. Ind. Electron.*, vol. 69, no. 4, pp. 3689–3699, Apr. 2022, ISSN: 0278-0046, 1557-9948. DOI: 10.1109/TIE.2021.3076721.
- [9] F. Xu, Z. Guo, H. Chen, D. Ji, and T. Qu, "A custom parallel hardware architecture of nonlinear Model-Predictive control on FPGA," *IEEE Trans. Ind. Electron.*, vol. 69, no. 11, pp. 11569–11579, Nov. 2022, ISSN: 0278-0046, 1557-9948. DOI: 10.1109/TIE.2021.3118427.
- [10] C. Gao, R. Gehlhar, A. D. Ames, S.-C. Liu, and T. Delbruck, "Recurrent neural network control of a hybrid dynamical trans-femoral prosthesis with EdgeDRNN accelerator," in *2020 IEEE International Conference on Robotics and Automation (ICRA)*, IEEE, May 2020, pp. 5460–5466. DOI: 10.1109/ICRA40945.2020.9196984.
- [11] F. Fahim, B. Hawks, C. Herwig, et al., "hls4ml: An Open-Source codesign workflow to empower scientific low-power machine learning devices," Mar. 2021. arXiv: 2103.05579 [cs.LG]. [Online]. Available: <http://arxiv.org/abs/2103.05579>.
- [12] J. L. Jerez, G. A. Constantinides, and E. C. Kerrigan, "An FPGA implementation of a sparse quadratic programming solver for constrained predictive control," in *Proceedings of the 19th ACM/SIGDA international symposium on Field programmable gate arrays*, 2011, pp. 209–218.
- [13] M. He and K.-V. Ling, "Model predictive control on a chip," in *2005 International Conference on Control and Automation*, vol. 1, IEEE, 2005, 528–532 Vol. 1, ISBN: 9780780391376. DOI: 10.1109/ICCA.2005.1528175.
- [14] K. V. Ling, S. P. Yue, and J. M. Maciejowski, "A FPGA implementation of model predictive control," in *2006 American Control Conference*, IEEE, 2006, 6 pp. ISBN: 9781424402090, 9781424402106. DOI: 10.1109/ACC.2006.1656502.
- [15] J. Liu, H. Peyrl, A. Burg, and G. A. Constantinides, "Fpga implementation of an interior point method for high-speed model predictive control," in *2014 24th International Conference on Field Programmable Logic and Applications (FPL)*, IEEE, 2014, pp. 1–8.
- [16] J. L. Jerez, G. A. Constantinides, and E. C. Kerrigan, "Fpga implementation of an interior point solver for linear model predictive control," in *2010 International Conference on Field-Programmable Technology*, IEEE, 2010, pp. 316–319.
- [17] J. L. Jerez, P. J. Goulart, S. Richter, G. A. Constantinides, E. C. Kerrigan, and M. Morari, "Embedded predictive control on an FPGA using the fast gradient method," in *2013 European Control Conference (ECC)*, IEEE, Jul. 2013, pp. 3614–3620, ISBN: 9783033039629. DOI: 10.23919/ECC.2013.6669598.
- [18] T. V. Dang, K. V. Ling, and J. M. Maciejowski, "Embedded ADMM-based QP solver for MPC with polytopic constraints," in *2015 European Control Conference (ECC)*, IEEE, 2015, pp. 3446–3451.
- [19] P. Zhang, J. Zambreno, and P. H. Jones, "An embedded scalable linear model predictive hardware-based controller using ADMM," in *2017 IEEE 28th International Conference on Application-specific Systems, Architectures and Processors (ASAP)*, IEEE, 2017, pp. 176–183.
- [20] A. Ravera, A. Oliveri, M. Lodi, and M. Storace, "MADS-based fast FPGA implementation of nonlinear model predictive control," in *2023 IEEE International Symposium on Circuits and Systems (ISCAS)*, IEEE, May 2023, pp. 1–5, ISBN: 9781665451093, 9781665451109. DOI: 10.1109/ISCAS46773.2023.10181647.
- [21] F. Diodati, B. Jeppesen, M. Jervis, and R. Saletti, "FPGA realization of a neural network based motor controller," in *2022 IEEE 27th International Conference on Emerging Technologies and Factory Automation (ETFA)*, IEEE, Sep. 2022, pp. 1–4, ISBN: 9781665499965, 9781665499972. DOI: 10.1109/ETFA52439.2022.9921591.
- [22] D. Wang, Z. J. Shen, X. Yin, S. Tang, J. Wang, and Z. Shuai, "Neural network based adaptive model predictive control for power converters under load parameter uncertainties," in *2022 4th International Conference on Electrical Engineering and Control Technologies (CEECT)*, IEEE, Dec. 2022, pp. 124–129, ISBN: 9781665498999, 9781665499002. DOI: 10.1109/CEECT55960.2022.10030277.
- [23] F. Dong, X. Li, K. You, and S. Song, "Standoff tracking using DNN-Based MPC with implementation on FPGA," *IEEE Trans. Control Syst. Technol.*, vol. 31, no. 5, pp. 1998–2010, Sep. 2023, ISSN: 1063-6536, 1558-0865. DOI: 10.1109/TCST.2023.3279115.
- [24] C. Gao, A. Rios-Navarro, X. Chen, S.-C. Liu, and T. Delbruck, "EdgeDRNN: Recurrent neural network accelerator for edge inference," *IEEE Journal on Emerging and Selected Topics in Circuits and Systems*, vol. 10, no. 4, pp. 419–432, Dec. 2020, ISSN: 2156-3365. DOI: 10.1109/JETCAS.2020.3040300.
- [25] F. Heetmeyer, M. Paluch, D. Bolliger, et al., "RPGD: A Small-Batch parallel gradient descent optimizer with explorative resampling for nonlinear model predictive control," in *2023 IEEE International Conference on Robotics and Automation (ICRA)*, IEEE, May 2023, pp. 3218–3224. DOI: 10.1109/ICRA48891.2023.10161233.
- [26] C. Green, *Equations of Motion for the Cart and Pole Control Task*, <https://sharpneat.sourceforge.io/research/cart-pole/cart-pole-equations.html>, Jan. 2020.
- [27] *Global race line trajectory optimizer*, Jul. 20, 2022. [Online]. Available: [https://github.com/TUMFTM/global\\_racetrjectory\\_optimization](https://github.com/TUMFTM/global_racetrjectory_optimization).
- [28] M. O’Kelly, H. Zheng, D. Karthik, and R. Mangharam, "FITENTH: An open-source evaluation environment for continuous control and reinforcement learning," in *NeurIPS 2019 Competition and Demonstration Track*, PMLR, 2020, pp. 77–89.
- [29] "CommonRoad-vehicle-models," TU München. (), [Online]. Available: <https://gitlab.lrz.de/tum-cps/commonroad-vehicle-models> (visited on 06/30/2021).
- [30] J. M. Snider et al., "Automatic steering methods for autonomous automobile path tracking," *Robotics Institute, Pittsburgh, PA, Tech. Rep. CMU-RITR-09-08*, 2009.
- [31] Y. Song, A. Romero, M. Müller, V. Koltun, and D. Scaramuzza, "Reaching the limit in autonomous racing: Optimal control versus reinforcement learning," en, *Sci Robot*, vol. 8, no. 82, eadg1462, Sep. 2023, ISSN: 2470-9476. DOI: 10.1126/scirobotics.adg1462.
- [32] A. Kumar, Z. Fu, D. Pathak, and J. Malik, "RMA: Rapid motor adaptation for legged robots," in *Robotics: Science and System XVII (RSS 2021)*, RSS Foundation, Jul. 2021. DOI: 10.15607/RSS.2021.XVII.011.
- [33] X. Chen, C. Gao, T. Delbruck, and S.-C. Liu, "EILE: Efficient incremental learning on the edge," in *2021 IEEE 3rd International Conference on Artificial Intelligence Circuits and Systems (AICAS)*, IEEE, Jun. 2021, pp. 1–4. DOI: 10.1109/AICAS51828.2021.9458554.